



Determination of the interparticle void volume in packed beds via intraparticle Donnan exclusion

Stephanie Jung, Steffen Ehlert, Martin Pattky, Ulrich Tallarek*

Department of Chemistry, Philipps-Universität Marburg, Hans-Meerwein-Strasse, 35032 Marburg, Germany

ARTICLE INFO

Article history:

Received 5 October 2009

Received in revised form

26 November 2009

Accepted 2 December 2009

Available online 5 December 2009

Keywords:

Packed beds

Packing density

Interparticle porosity

Donnan exclusion

Inverse size-exclusion chromatography

Pore blocking

ABSTRACT

Interparticle void volumes and porosities of packed capillaries have been determined using intraparticle Donnan exclusion of a small, unretained, co-ionic tracer (nitrate ions). The operational domain of this approach has been characterized for bare silica, reversed-phase, and strong cation-exchange materials (with different particle sizes and intraparticle pore sizes) in dependence of the mobile phase ionic strength. Interparticle porosities agree well with those analyzed by inverse size-exclusion chromatography (ISEC). Limitations to the use of Donnan exclusion (electrostatic exclusion) and ISEC (mechanical exclusion) arise as either type of exclusion becomes noticeable also in the cusp regions between the particles, or as the intraparticle pores are so large that complete electrostatic and size-exclusion are difficult to realize. Our data confirm that intraparticle Donnan exclusion presents a most simple, fast, and reliable approach for the analysis of packing densities.

© 2009 Elsevier B.V. All rights reserved.

1. Introduction

The measurement and meaning of void volumes in reversed-phase liquid chromatography (RPLC) have been the subject of a considerable number of publications, as reviewed a few years ago by Rimmer et al. [1] and, consequently, have been studied extensively from theoretical and experimental point of views [2]. The total volume of a particle-packed RPLC column can be written as the sum of three contributions: (i) the interparticle, interstitial, or external pore volume; (ii) the intraparticle or internal pore volume; and (iii) the unaccessible volume which can be split into the stationary-phase solid volume, the closed-pore volume, and the volume of the bonded chains [3]. The different void volumes of a packed column are important in both kinetic and thermodynamic measurements, particularly when attempts are made to correlate solute retention with solvent composition [4,5].

In this work we are concerned with the interparticle void volume (V_{inter}) and porosity ($\varepsilon_{\text{inter}}$). Its accurate determination and the corresponding analysis of packing densities provides essential feedback, e.g., during the optimization of column packing conditions and dynamic bed consolidation [6–9], or in the discussion of hydraulic permeabilities via phenomenological models

and so-derived correlations [10]. This is reflected in the strong dependence on $\varepsilon_{\text{inter}}$ of different porosity functions that have been used to characterize the resistance to low Reynolds number flow of liquid through packed beds, including the most popular one $(1 - \varepsilon_{\text{inter}})^2 / \varepsilon_{\text{inter}}^3$ after Blake, Kozeny, and Carman, or $4(1 - \varepsilon_{\text{inter}})\varepsilon_{\text{inter}}^{-4.55}$ after Rumpf and Gupta which appears to be more accurate [11].

Traditionally, V_{inter} (and $\varepsilon_{\text{inter}}$) in packed beds are analyzed by inverse size-exclusion chromatography (ISEC) [12]. While classical SEC uses the known pore structure of an adsorbent to determine the molecular weight distribution of a polymer mixture [13], the pore size distribution of an unknown stationary-phase can be determined from the distribution of retention volumes of a series of polymer standards if their molecular weight is known. Provided that standard samples are available for calibration, experiments show that there exists a correlation between the average molecular weight of the polymers and average diameter of the pores from which they are excluded, assuming that all polymeric chains remain in the same conformation of a random coil [13]. For each packing material, there are two thresholds, a low and a high one. Molecules larger than the high threshold have no access to any significant fraction of the intraparticle porosity. Molecules smaller than the low threshold have access to the entire pore volume. In ISEC solutions of known polymeric samples are injected into a column packed with an unknown adsorbent, and the retention behavior of these solutes can be correlated with the pore size distribution of the packing material [3,12]. Plots of the logarithm of the molecular weight

* Corresponding author. Tel.: +49 6421 28 25727; fax: +49 6421 28 22124.

E-mail address: tallarek@staff.uni-marburg.de (U. Tallarek).

URL: <http://www.uni-marburg.de/fb15/ag-tallarek> (U. Tallarek).

of the polystyrenes versus their retention time reveal a bimodal pore size distribution representing the internal (intraparticle) and external (interparticle) porosity of the packed bed.

To overcome drawbacks of ISEC for the analysis of V_{inter} (and $\varepsilon_{\text{inter}}$) in packed beds [14] Cabooter et al. [15] recently presented a method that relies on measuring the elution time of an unretained small tracer after having filled the intraparticle pores of the particles with a hydrophobic solvent that is completely immiscible with the mobile phase employed during the elution time measurements. Thus, based on the total blocking of the intraparticle pores in a packed bed it allows to perform interparticle void volume measurements with a single, small tracer rather than a large polymer standard. While the total pore blocking method requires careful, time-consuming pretreatment of the materials, it does not need the regression analysis underlying ISEC.

Another and at least as accurate, but far simpler method than total pore blocking and ISEC for the analysis of V_{inter} (and $\varepsilon_{\text{inter}}$) in packed beds is based on the interparticle elution of organic or inorganic ions which are completely, but in this case electrostatically excluded from the intraparticle pore space due to the Donnan potential [16–18]. This approach originates as a limiting variant of the much explored use of organic or inorganic ions as dead time markers in RPLC (see Chapter 4.3 in [1] and references therein). In this context, it has been noted that mobile phases and/or samples with sufficient ionic strength are required to effectively screen the surface charges of the intraparticle pores and prevent Donnan exclusion of the charged dead time markers (which behave co-ionic with respect to the surface charge). As, towards the opposite electrostatic extreme, mobile phase composition is tuned for complete intraparticle Donnan exclusion (i.e., at sufficiently low ionic strength) a small, unretained, co-ionic tracer permeates through the interparticle void space only. It allows the fast, non-invasive analysis of V_{inter} (and $\varepsilon_{\text{inter}}$) using water-soluble, UV-detectable ions such as nitrate.

The use of simple organic or inorganic ions as selective markers for V_{inter} (and $\varepsilon_{\text{inter}}$) in packed beds based on the intraparticle Donnan exclusion has been observed and explored before [4,14,17,19–23]. In this work, we present further insight into the operational domain of this simple as elegant approach by addressing, together with a variation of the mobile phase ionic strength, the influence of the intraparticle mean pore size and surface charge density, as well as the onset of Donnan exclusion already on the interparticle pore level in dependence of the mean particle size. Values of $\varepsilon_{\text{inter}}$ are compared with those obtained by the traditional ISEC method.

2. Background

In porous adsorbents like membranes, sphere packings, and monoliths which contain charged solid–liquid interfaces and through which ionic species (simple ions, analytes, or colloidal particles) are transported, several electrical fields may be superimposed. This includes local fields near the wall of charged pores, or around devised spacer groups and bonded chains which extend from the surface, the Donnan potentials between different compartments in hierarchically structured materials, the quasi-equilibrium electrical double-layer (EDL) at the phase boundaries, as well as externally applied fields [18,24].

Ion-permselectivity (charge-selectivity) is a unique and often tailored characteristic of porous media which they can show either as a whole (e.g., membranes separating completely adjacent solutions) or by means of local, discrete ion-permselective regions (meso- and/or microporous domains) in materials which are macroscopically charge-nonspecific (packed beds, monoliths). While charge-selectivity traditionally plays a central role in membrane science [25,26], ion-permselective transport also prevails

in the intraparticle or intraskelton mesopores of particulate and monolithic columns typically used in HPLC (Fig. 1) [17,18]. It is therefore also relevant to reversed-phase silica particles, even those with a conventional endcapping, due to the persistence of residual silanol groups which, in turn, contribute a pH-dependent surface charge [27].

The characteristic pore sizes d_{pore} of the interparticle (interskeleton) macropore space of a packed bed (monolith) usually substantially exceed the typical EDL thickness δ_{EDL} at the particles external surface (along the monolith skeleton), as illustrated in Fig. 1A ($d_{\text{pore}} \gg \delta_{\text{EDL}}$). Thus, liquid in the macropore space is quasi-electroneutral (thin-EDL-limit) and transport numbers of the co-ions and counterions in the background electrolyte are well balanced. By contrast, intraparticle or intraskelton mesopore sizes are comparable with the EDL thickness (Fig. 1A, $d_{\text{pore}} \approx \delta_{\text{EDL}}$), as shown in Fig. 1B for a representative silica-based monolith and a packed bed [24]. The mesopore-scale EDL interaction (also referred to as EDL overlap) results in counterion enrichment and co-ion exclusion with respect to the bulk solution. As illustrated in Fig. 2 it is governed by the surface electrical potential inside the mesopores (ψ_s) and $r_{\text{pore}}/\lambda_D$, the ratio of the intraparticle or intraskelton mesopore radius r_{pore} (if we assume cylindrical pores for simplicity) and the Debye screening length λ_D which characterizes the EDL thickness and which depends on the mobile phase ionic strength according to [28]

$$\lambda_D = \left(\frac{\varepsilon_0 \varepsilon_r RT}{F^2 \sum_i z_i^2 c_{i,\infty}} \right)^{1/2}, \quad (1)$$

where ε_0 and ε_r are the permittivity of vacuum and relative permittivity of the bulk solution, respectively. R is the gas constant, T is the absolute temperature, and F is the Faraday constant; z_i is the valency of ionic species i and $c_{i,\infty}$ its concentration in the electroneutral, bulk solution (that is, beyond the EDL).

Depending on the actual intensity of EDL overlap, e.g., inside mesoporous particles of a packed bed represented by $r_{\text{pore}}/\lambda_D$, we expect the complete permeation ($\varepsilon_{\text{tracer}} = \varepsilon_{\text{total}}$) and exclusion ($\varepsilon_{\text{tracer}} = \varepsilon_{\text{inter}}$ only) of an unretained, co-ionic tracer as the extreme scenarios (Fig. 2) [17,19,20,23]. For $r_{\text{pore}}/\lambda_D \approx 1$, the EDL extends over the whole pore fluid; the pore is ion-permselective and excludes co-ions. Their transport numbers decrease at increasing EDL overlap, while those of the counterions increase. For $r_{\text{pore}} \gg \lambda_D$, the EDL is confined to a thin layer at the pore walls only, meaning that the whole pore fluid is quasi-electroneutral and its charge-selectivity disappears. The transport numbers of co-ions and counterions become balanced. These extremes ($r_{\text{pore}}/\lambda_D < 1$ and $r_{\text{pore}}/\lambda_D \gg 1$) and the broad intermediate regime can be easily tuned in chromatographic practice by the mobile phase ionic strength ($\rightarrow \lambda_D$) and the intraparticle pore dimensions ($\rightarrow d_{\text{pore}}$). Apart from ion-exclusion chromatography, this adjustable electrostatic on-off behaviour [18,29–34] of the intraparticle permeation in chromatographic media (Fig. 2) is relevant also for the design of preparative separations and purification processes [35–38], because the actual electrolyte concentration determines the availability of chromatographic sites and “effective porosity” for co-ionic analytes, as well as the pore-level concentrations of charged analytes (co-ion exclusion, counterion enrichment), in general.

Alternatively, the situation illustrated by Figs. 1 and 2 can be analyzed in terms of Donnan exclusion [16]. At electrochemical equilibrium between electrolyte solutions in both compartments (Fig. 1A) the counterion concentration in the intraparticle (intraskelton) mesopore space is higher and the co-ion concentration lower than in the interparticle (interskeleton) macropore space. An electrical phase boundary potential between interconnected bulk and ion-permselective domains balances the tendency of ions to level out these concentration (chemical potential) differ-

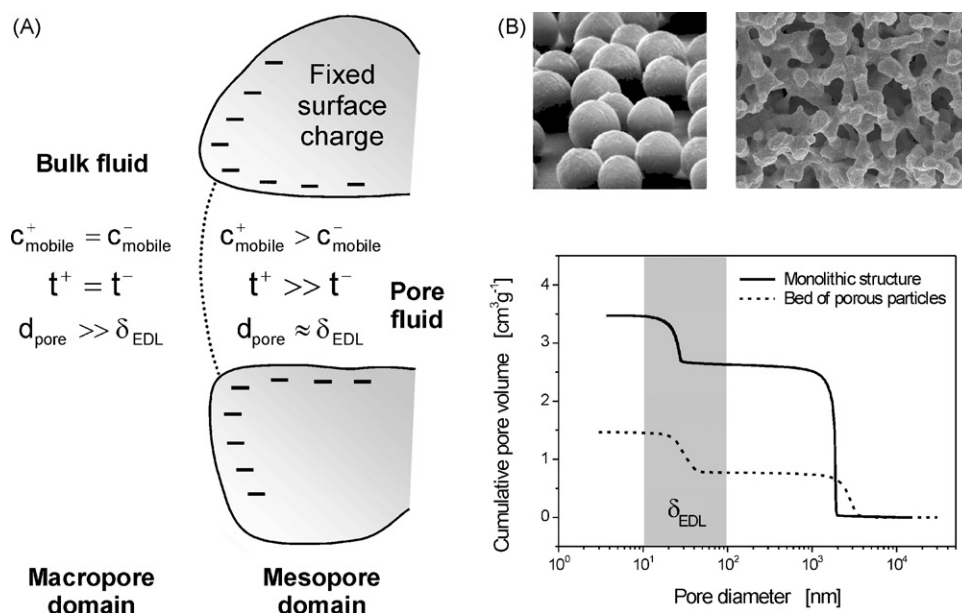


Fig. 1. (A) Schematic representation of equilibrium ion concentrations (for a strong, symmetrical background electrolyte), transport numbers, and the ratio of the local pore diameter (d_{pore}) to the EDL thickness (δ_{EDL}) in the interconnected macropore and mesopore spatial domains of hierarchically structured materials. The concentration of mobile counterions (c_{mobile}^+) and their transport number (z^+t^+ ; t^+ is the transference number [16]) in the pore fluid of the mesopore domain exceed those of the co-ions. (B) Scanning electron microscopy images and pore size distributions characterizing many sphere packings and monolithic structures. These fixed beds reveal bimodal pore size distributions due to intraparticle (intraskeleton) mesopores and interparticle (interskeleton) macropores. Reprinted with permission from Leinweber et al. [24]. Copyright 2005 American Chemical Society.

ences. This potential is also known as the Donnan potential (Φ_{Don}) [39,40]. It pulls cations back into the negatively charged intraparticle (intraskeleton) pore space and anions back into the positively charged interparticle (interskeleton) compartment [41]. For ideal solutions we have

$$\Phi_{Don} \equiv \phi_{intra} - \phi_{inter} = -\frac{RT}{z_i F} \ln \frac{c_{i,intra}}{c_{i,inter}}, \quad (2)$$

where i applies to TrisH^+ , H_3O^+ , and K^+ ($z_i = +1$) as well as to Cl^- , OH^- , and NO_3^- ($z_i = -1$) for the buffer (Tris-HCl) and tracer salt (KNO_3) used in the present work. The distribution coefficient $c_{i,intra}/c_{i,inter}$ (which represents the ion-permeability of the particles or the monolith skeleton) depends on the mobile phase ionic strength, the surface charge density in the intraparticle or intraskeleton pore space, and the valencies of the co-ionic and

counterionic species. Actually, these parameters similarly influence EDL overlap and resulting co-ion exclusion (counterion enrichment) in a double-layer model.

The considerations on relevant parameters (Figs. 1 and 2) which define the operational domain of co-ion exclusion and inorganic ions as selective markers for V_{inter} (and ε_{inter}) in packed beds have motivated us to conduct the following capillary HPLC experiments. For an extended range of mobile phase ionic strengths (Tris-HCl buffer) and with KNO_3 as the tracer salt we compared particles with similar intraparticle mean pore sizes, but different surface charge densities (reversed-phase, bare silica, strong cation-exchange); particles with different intraparticle pore sizes (100 and 1000 Å); as well as different mean particle sizes (3, 5 and 10 μm) to retrieve Donnan exclusion not only inside, but already between the particles.

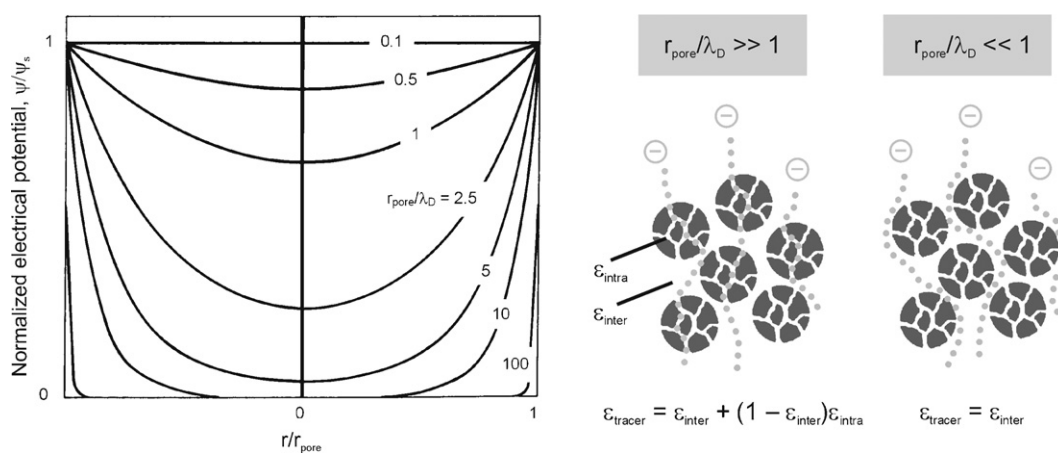


Fig. 2. Pore-scale distribution of electrical potential normalized by the surface potential ψ_s for different values of r_{pore}/λ_D reflecting EDL overlap and co-ion exclusion (adapted from [28]). For $r_{pore}/\lambda_D \gg 1$ a co-ionic (here negatively charged) tracer has access to the total porosity of the packed bed, while for $r_{pore}/\lambda_D \ll 1$ it samples only the interparticle porosity. Plots of the elution volumes of a co-ionic tracer versus r_{pore}/λ_D reveal a bimodal pore size distribution with a plateau region at low ionic strength representing the interparticle porosity and another plateau region at high ionic strength where the charge-selectivity of the particles has disappeared and the co-ionic tracer experiences the entire pore space.

3. Experimental

3.1. Chemicals and materials

Organic solvents of HPLC-grade (acetonitrile, methylene chloride, methanol, ethanol, and acetone) were purchased from Sigma–Aldrich (Taufkirchen, Germany). Benzene and KNO_3 were obtained from Carl Roth (Karlsruhe, Germany). Hydrochloric acid was bought from VWR International (Briare, France). Polystyrene standards with a molecular weight of 2500, 5000, 9000, 30,000 and 50,000 g/mol were purchased from Supelco (Bellefonte, PA). Polystyrene standards with 20,000, 100,000, 500,000, 1,000,000, 2,000,000, and 4,000,000 g/mol as well as Tris(hydroxymethyl)aminomethane came from Fluka Chemie (Buchs, Switzerland). HPLC-grade water was prepared with a Milli-Q gradient water purification system (Millipore, Bedford, MA).

In our capillary HPLC studies we employed the following support particles: 3- and 10- μm sized 120 Å Hypersil MOS (monomeric octyl silica, C8) (Thermo Fisher Scientific, Waltham, MA); 3- μm sized 80 Å Spherisorb SCX (propanesulfonic acid-modified silica) (Waters, Milford, MA); and 5- μm sized 100 Å and 1000 Å Nucleosil 100-5 and Nucleosil 1000-5 (bare silica) (Macherey–Nagel, Düren, Germany). These particles were slurry-packed into 75 μm i.d., 360 μm o.d. cylindrical fused-silica capillaries (Polymicro Technologies, Phoenix, AZ).

3.2. Apparatus

All data were acquired with an Agilent 1100 liquid chromatograph (Agilent Technologies, Waldbronn, Germany) consisting of a degasser and a nanopump, equipped with a variable wavelength UV detector (VWD) and a high-sensitivity cell (SunChrom, Friedrichsdorf, Germany) working at 254 nm for the ISEC experiments with the polystyrene standards and at 210 nm for the Donnan exclusion experiments with KNO_3 . Manual sample injection was performed via a two-position injection valve with a 4 nl internal loop volume (Model CN4 from Vici AG Valco Europe, Schenkon, Switzerland). The loop was continuously flushed by use of a syringe installed on a syringe pump (Harvard Apparatus, Holliston, MA). Fused-silica restriction capillaries having a length of either 900 mm (15 μm i.d.) or 500 mm (10 μm i.d.) were used as pre-columns to ensure a sufficient working pressure. Volumetric flow rates were continuously monitored by an external flow sensor (Model SLG-1430-150, Sensirion, Stäfa, Switzerland) connected to the outlet of the detection cell. To avoid daily fluctuations of the nanopump the actual flow rates recorded by the external flow sensor were used to calculate elution volumes of the analytes. All experiments were carried out at 298 ± 1 K under isocratic elution conditions. Injections were thrice-repeated for a given capillary and the results averaged to account for the error from manual injection.

3.3. Capillary packing

Capillaries were slurry-packed using a WellChrom K-1900 pneumatic pump (Knauer, Berlin, Germany) with a 500 μm i.d. glass-lined metal tubing as the slurry reservoir [8,42]. A micro-union with a 1 μm mesh stainless-steel frit (IDEX Health & Science, Wertheim-Mondfeld, Germany) was connected to each capillary to provide a temporary outlet frit during packing. Slurries were prepared by suspending the dry particles in 1 ml of the appropriate solvent while applying ultrasound for 10 min (Table 1).

The degassed pushing (packing) solvents were also used for rinsing and conditioning of the fused-silica capillaries prior to the packing process. The packing process was then started by injecting 70 μl of the prepared slurries into the reservoir and applying 300 bar pressure for at least 5 min to transport the respective slurry

into the capillary. After a short optical inspection to verify whether the packing of the capillary had started or blockage occurred, the pressure was raised (Table 1) and the capillaries were inserted into an ultrasonic bath (Bandelin Electronic, Berlin, Germany) for 40 min during packing and consolidation. As demonstrated earlier the application of ultrasound appeared to be critical for obtaining densely packed capillaries [8].

After consolidation of the packing, the system was depressurized slowly and the capillary removed from the packing device. The pushing solvent was replaced by bidistilled, filtered, and degassed water containing NaCl which was needed for preparing mechanically stable frits (Table 1). Afterwards, the capillary was reassembled within the packing device and flushed for 90 min with the aqueous electrolyte solution for a complete exchange of the packing solvent. The bed was fixed by a sintered inlet and outlet frit to obtain a total bed length of about 120 mm. The packed capillaries were cut off at the frits with a capillary column cutter (Shortix™ from SGT Middelburg B.V., The Netherlands) and connected to the injector using optimized fittings (Nanovolume™ from Vici AG Valco Europe, Schenkon, Switzerland). This experimental set-up allowed dead volume-free injection onto the packed beds. The capillary outlet frit was connected to the detector inlet with a zero-dead-volume adapter (Micro Tight ZDV P-770 from IDEX Health & Science, Wertheim-Mondfeld, Germany). Packing procedures were not evaluated for separation efficiencies; the conditions in Table 1 proved to be adequate for obtaining stable packed beds without gaps and further tendency for settling during the measurements.

3.4. Porosity measurements

Interparticle void volumes and porosities (V_{inter} and $\varepsilon_{\text{inter}}$) of the packed capillaries were analyzed by ISEC (size-exclusion) and Donnan (electrostatic) exclusion. In the former case benzene (1 mmol/l) and a total of eleven polystyrene standards ranging from 2500 to 4,000,000 g/mol (0.6 mg/ml each) were dissolved in methylene chloride. Analytes were injected and chromatographed at a flow rate of 200 nl/min and detection at 254 nm. For the determination of V_{inter} and $\varepsilon_{\text{inter}}$ via Donnan exclusion in capillaries packed with the Hypersil MOS phases KNO_3 in 70/30 acetonitrile/water (v/v) was injected and detected at 210 nm. For the bare silica and SCX materials KNO_3 was used in 30/70 acetonitrile/water (v/v). The concentration of Tris–HCl buffer (pH 8.1) in the mobile phases was varied from 0.01 to 40 mM and is, where useful, also presented as λ_D (the Debye screening length, Eq. (1)) to express the Donnan exclusion of nitrate via $r_{\text{pore}}/\lambda_D$ (cf. Fig. 2). The relative permittivity (ε_r) in Eq. (1) for the mobile phases was taken from Moreau and Dohéret [43].

For low buffer concentrations in the running mobile phase (from 0.01 to 0.1 mM) just pure KNO_3 solutions (in the respective, but unbuffered mobile phase) were employed for sample injection. In this case, the KNO_3 concentration was adjusted to the ionic strength of the running mobile phase, which was found to result in negligible disturbances of the intraparticle Donnan exclusion during elution of the nitrate due to the mismatch between injected sample and running mobile phase. At higher buffer concentrations (>0.1 mM) a fixed KNO_3 concentration of 0.04 mM was added to the respective and now buffered mobile phase for sample injection.

To obtain accurate elution volumes from the elution times of the analytes, the actual flow rate as permanently monitored by the external flow sensor had to be employed. This procedure turned out to be necessary because the pump flow varied with the temperature of the nanopump (which increased during daily running time). The results were corrected for the dead volume, which was measured by connecting the detector inlet directly to the injection valve. The elution volume of an analyte obtained with this set-up equals the

Table 1
Packing conditions for the adsorbents.

Packing material	Slurry solvent	Slurry concentration	Packing solvent	Max. applied pressure	Fritting electrolyte
Hypersil MOS; 3 μm , 120 Å	Acetone	20 mg/ml	Methanol	550 bar	1 g/l NaCl
Hypersil MOS; 10 μm , 120 Å	Acetone	20 mg/ml	Methanol	550 bar	1 g/l NaCl
Spherisorb SCX; 3 μm , 80 Å	1 M NaCl	10 mg/ml	2 M NaCl	550 bar	30 g/l NaCl
Nucleosil; 5 μm , 100 Å	Ethanol	35 mg/ml	Water	400 bar	1 g/l NaCl
Nucleosil; 5 μm , 1000 Å	Ethanol	15 mg/ml	Water	300 bar	1 g/l NaCl

internal volume of the detector capillary and therewith the overall dead volume.

4. Results and discussion

Interparticle void volumes and porosities (V_{inter} and $\varepsilon_{\text{inter}}$) have been determined by ISEC and via Donnan exclusion for all packings. In ISEC eleven polystyrene standards with molecular weights (M_W) from 2500 to 4,000,000 g/mol and benzene dissolved in methylene chloride were injected onto the packed capillaries for each packing material. Interparticle porosities ($\varepsilon_{\text{inter}} = V_{\text{PS}}/V_{\text{column}}$) were calculated from the elution volumes of the most suitable standard (V_{PS}), which is just size-excluded from the intraparticle pore space, and the geometrical column volume (V_{column}). The latter has been determined by measuring the nitrate elution volumes for the empty capillaries that were subsequently used for packing.

It should be mentioned that the elution volume of even the smallest (yet completely size-excluded) polystyrene standard is expected to differ from the real morphological interparticle void volume of the packing. Depending on its finite size an analyte like the polystyrene standard intrinsically has a reduced access to the interparticle pore space compared with a fictitious “point mass analyte” [44]. To ensure that the so-derived values of $\varepsilon_{\text{inter}}$ are not falsified by the actual molecular size of the identified polystyrene standard we complementary plotted the elution volumes of all polystyrene standards against the cubic root of their molecular weight (Fig. 3) [45]. Employing the elution volumes of only the size-excluded polystyrene standards the intersection with the ordinate for “zero molecular weight” ($M_W^{1/3} = 0$) reflects the morphological interparticle void volume experienced by a fictitious “point mass analyte” and can be calculated via linear regression (see Fig. 3). $\varepsilon_{\text{inter}}$

is then recalculated from this maximal V_{inter} (intersection with the ordinate) and V_{column} . Under the conditions of the present study differences in V_{inter} were only on the order of 1–3%. According corrections to the values of $\varepsilon_{\text{inter}}$ based on the elution volumes of the most suitable polystyrene standard thus remained insignificant. This result can be rationalized by considering the large interparticle pore dimensions of the packings made of 3 or 10 μm particles [46] with respect to the size of the smallest polystyrene standard that is completely size-excluded from their mesopores and used for the determination of V_{inter} (Fig. 3).

Plots of $\log(M_W)$ of the polystyrene standards versus their elution volume revealed a bimodal pore size distribution for all packings. Only for capillaries packed with macroporous Nucleosil 1000-5 material the determination of the high threshold was not unambiguous, as discussed later. The intersection of the calibration curves providing the smallest polystyrene coil which is completely excluded from the intraparticle pore space was determined graphically by regression. The associated pore diameter of each stationary-phase was calculated with [12]:

$$d_{\text{pore}}[\text{Å}] = 0.62(M_W)^{0.59} \quad (3)$$

and values are summarized in Table 2. Halász and Martin [12] found that the pore diameter of a solid assigned by Eq. (3) to a polystyrene of molecular weight M_W dissolved in methylene chloride is 2.5 times larger than the rotational coil diameter of the same polystyrene molecule. They introduced the factor of 2.5 to fit their SEC data to the mean pore diameter found by classical methods. Thus, Halász and Martin [12] shifted the SEC curves to mean pore diameters 2.5 times larger than the rotational coil diameter. The so-obtained “new” pore size distribution bears little relation to the pore size distribution derived by mercury porosimetry or computational approaches [47], but it provides a reasonable value for the mean pore diameter [47]. Although the pore diameters calculated with Eq. (3) (Table 2) should be taken with caution, they enable a comparison with manufacturers’ data and the other silica-based materials used in this work.

When comparing the results in Table 2 with the manufacturers’ data only slight differences are resolved for Hypersil MOS and Spherisorb SCX particles. For the Nucleosil 100-5 particles the calculated pore diameter turned out to be significantly higher (162 Å instead of the nominal 100 Å); similarly, the 2,000,000 g/mol polystyrene standard denotes $d_{\text{pore}} = 1295$ Å for the Nucleosil 1000-5 particles (nominal $d_{\text{pore}}: 1000$ Å). Although the determined pore diameters of the Nucleosil particles deviate from the manufacturers’ data the resulting ratio of ~ 8 (Nucleosil 1000-5 to Nucleosil 100-5) is at least comparable with the nominal ratio of 10.

Interparticle porosities determined by Donnan exclusion were calculated from the nitrate elution volumes at a buffer concentration of 0.02 mM, where elution volumes (V_{tracer}) for most packings reached the plateau region (see below) indicating complete intraparticle Donnan exclusion, and the geometrical column volume (V_{column}). To realize maximum surface charge of all packing materials the aqueous part of all mobile phases was buffered with Tris-HCl (pH 8.1). This caused a complete dissociation of silanol groups on the surface of the bare silica, reversed-phase silica, and SCX particles.

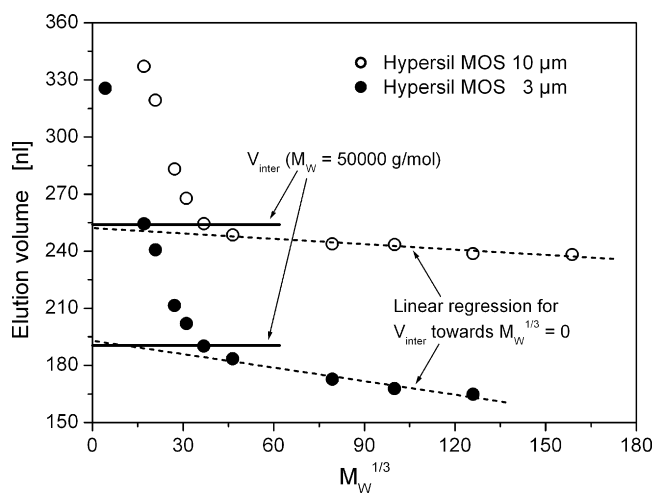


Fig. 3. Elution volumes of polystyrene standards vs. the cubic root of their molecular weight. Linear regression for size-excluded polystyrene standards towards $M_W^{1/3} = 0$ (dotted lines) determines the maximal interparticle void volume V_{inter} of capillaries packed with the 3 and 10- μm sized Hypersil MOS particles (120 Å nominal pore size) which would be experienced by a size-excluded, but fictitious “point mass analyte”. The solid lines denote the real elution volumes of the smallest size-excluded polystyrene standard ($M_W = 50,000$ g/mol).

Table 2
Characteristics of the packed capillaries.

Packing material	ISEC approach d_{pore} [Å]	ISEC approach ϵ_{inter} (PS)	Donnan exclusion ϵ_{inter} (NO_3^-)
Hypersil MOS; 3 μm , 120 Å	110	0.36	n.a.
Hypersil MOS; 10 μm , 120 Å	119	0.41	0.42
Spherisorb SCX; 3 μm , 80 Å	95	0.43	0.42
Nucleosil; 5 μm , 100 Å	162	0.44	0.43
Nucleosil; 5 μm , 1000 Å	1295	n.a.	<0.49

Interparticle porosities are summarized in Table 2 and show good agreement between the two methods (ISEC and Donnan exclusion). Packing densities for the Hypersil MOS phases with $\epsilon_{\text{inter}} = 0.36$ for the 3 μm and $\epsilon_{\text{inter}} = 0.41\text{--}0.42$ for the 10 μm particles at a particle-aspect ratio (column-to-particle diameter ratio) of $d_c/d_p = 25$ and 7.5, respectively, agree with the trend in earlier investigations where the packing density of confined cylindrical beds was found to decrease exponentially at low particle-aspect ratios due to the increasing contribution of the geometrical wall effect [8,48]. The value of $\epsilon_{\text{inter}} = 0.36$ realized with the 3 μm Hypersil MOS particles closely reflects the maximum density of disordered (random) hard sphere packings [49,50]. The Nucleosil bare silica particles were packed at lower pressures to avoid damage of the highly porous particle structure (Table 1). The application of high packing pressures turned out to be essential for the generation of densely packed beds, thus the lower packing pressures limited by the stability of the Nucleosil material explain the slightly higher porosities of the Nucleosil 100-5 ($\epsilon_{\text{inter}} = 0.43\text{--}0.44$) and Nucleosil 1000-5 ($\epsilon_{\text{inter}} < 0.49$) packings. Additionally, the Nucleosil particles revealed a stronger deviation from spherical shape and a higher surface roughness than the other materials which also contributes to lower packing densities [8,51].

Despite these obvious differences in packing densities all packings were consolidated, rigid, and therefore met the requirements for a reliable data acquisition by chromatographic measurements of the interparticle void volumes. Careful microscopic inspection revealed that all packings remained densely packed; no voids were observed in the axial direction before and after the chromatographic analysis.

4.1. Effect of the mean particle size

Fig. 4 shows the calibration curves for electrostatic exclusion (Fig. 4A) and size-exclusion (Fig. 4B) acquired with the Hypersil MOS particles (120 Å nominal pore size). Comparing the calibration curves for the two differently sized materials ($d_p = 3$ and 10 μm nominal particle size) it is first noticed that both size-exclusion and Donnan exclusion with the 10 μm particles develop relatively discretely. Complete Donnan exclusion in Fig. 4A (open circles) is characterized by the plateau region at low buffer concentrations where the normalized elution volumes $V_{\text{tracer}}/V_{\text{column}}$ are plotted versus the dimensionless ratio $r_{\text{pore}}/\lambda_D$ characterizing intraparticle EDL overlap (or Donnan exclusion). In the plateau region nitrate is completely excluded from the negatively charged intraparticle pore space (thus, $V_{\text{tracer}} \equiv V_{\text{inter}}$). This exclusion persists up to $r_{\text{pore}}/\lambda_D = 0.12$ (which translates to a Tris buffer concentration of 0.04 mM) and these “plateau” elution volumes can be used for calculating the interparticle porosity according to $\epsilon_{\text{inter}} = V_{\text{inter}}/V_{\text{column}}$. At higher ionic strength nitrate ions begin to penetrate the intraparticle pore space (and $V_{\text{tracer}} > V_{\text{inter}}$). The hyperbolic shape of the graph in Fig. 4A (open circles) results from the inverse dependence of λ_D on the square root of the counterion concentration (Eq. (1)), so that the electrostatic (Donnan) exclusion is only slowly developing (or disappearing) over a wide range of mobile phase ionic strengths. At the highest buffer concentration (40 mM) the nitrate ions are still not able to penetrate the

complete pore space; otherwise, the elution volumes would reach a second plateau (where $V_{\text{tracer}} \equiv V_{\text{total}}$). This illustrates that relatively high ionic strengths need to be realized in order to use the nitrate ions as a tracer for the column dead volume [1,17]. The size-exclusion curve for the 10 μm Hypersil MOS particles (Fig. 4B, open circles) reveals a bimodal distribution. Benzene has access to the entire pore space and it therefore denotes the overall void volume of the packing. Complete size-exclusion is reached with the polystyrene standard of 50,000 g/mol (cf. Fig. 3). With further increasing molecular weight of the polystyrene standards a sharp increase in slope is observed leading to a nearly vertical calibration curve.

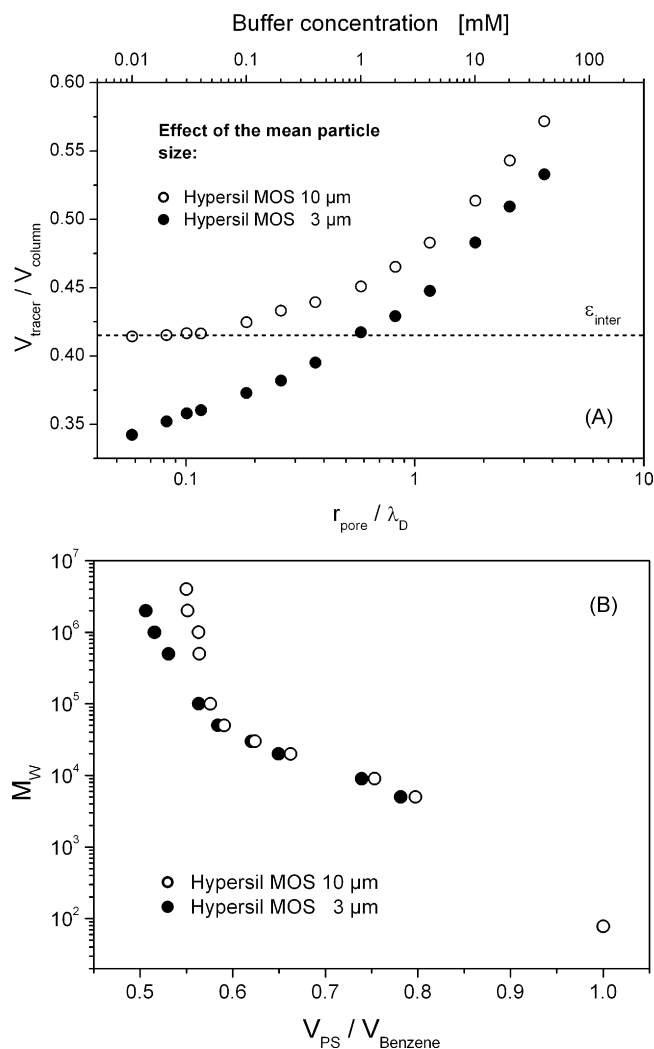


Fig. 4. (A) Electrostatic exclusion curves of nitrate vs. $r_{\text{pore}}/\lambda_D$ and (B) inverse size-exclusion curves of polystyrene standards with known molecular weight (M_W) for capillaries packed with the 3- and 10- μm sized Hypersil MOS particles (120 Å nominal pore size). The elution volumes of nitrate (V_{tracer}) were normalized by the empty capillary volume (V_{column}), while polystyrene elution volumes (V_{PS}) were normalized by that of benzene.

Calibration curves for electrostatic and size-exclusion in the case of capillaries packed with the smaller (3- μm sized) Hypersil MOS particles reveal a different trend. The Donnan exclusion curve in Fig. 4A at high ionic strengths (and, correspondingly, high values of $r_{\text{pore}}/\lambda_{\text{D}}$) is similar to the calibration data for the 10 μm particles with a nearly identical surface chemistry and pore size distribution; however, at decreasing ionic strength (and decreasing $r_{\text{pore}}/\lambda_{\text{D}}$) $V_{\text{tracer}}/V_{\text{column}}$ does not enter into a plateau region. Instead, the nitrate elution volumes continue to decrease. To explain this behavior, another aspect of packing morphology needs to be considered. Compared with the $d_{\text{p}}=3\ \mu\text{m}$ packings the 10 μm packings not only consist of larger particles (translating to larger $d_{\text{p}}/\lambda_{\text{D}}$ ratios), but they are also more loosely packed (cf. Table 2). The mean nearest-neighbor distance in random sphere packings depends on the packing density [46]. As a result (concerning absolute particle size and packing density), significant EDL overlap does not develop between the loosely packed 10 μm particles, even as the EDL thickness continues to increase at decreasing buffer concentration. By contrast, EDL overlap in the interparticle pore space becomes important for the densely packed 3 μm packings and explains the continued decrease in nitrate elution volumes at decreasing $r_{\text{pore}}/\lambda_{\text{D}}$ (without entering a plateau). In other words, while still increasingly excluded from the intraparticle pore space the nitrate ions already become partly excluded (electrostatically) from the interparticle pore space as well.

The relevance of the interparticle pore space dimensions is also reflected in the ISEC graphs (Fig. 4B), but now in view of size-exclusion, not electrostatic exclusion. For the densely packed 3 μm packings the high- M_{W} polystyrenes indicate a stronger exclusion from parts of the interparticle void space than in the loosely packed 10 μm packings. The smaller slope in Fig. 4B for the size-excluded polystyrenes in case of the 3 μm packings can be explained by the onset of size-exclusion from the interparticle pore space already where these polystyrenes are unable to fully penetrate the cusp regions between the small (and densely packed) 3 μm particles. However, as we have shown in Fig. 3 this effect remains negligible for the smallest size-excluded polystyrene ($M_{\text{W}}=50,000\ \text{g/mol}$) which is used in the determination of V_{inter} and $\varepsilon_{\text{inter}}$ by ISEC.

4.2. Effect of the surface charge density

To study the influence of the intraparticle surface charge density on Donnan exclusion nitrate elution curves for the 3 μm Hypersil MOS particles and 3 μm Spherisorb SCX particles are compared in Fig. 5A. Both particles have similar intraparticle pore sizes (110 and 95 \AA , Table 2), but their surface modification is very different. Hypersil MOS is a dimethyloctylsilane non-encapped silica, whereas the Spherisorb SCX is a propanesulfonic acid-modified silica. By comparing calibration curves in Fig. 5A, where normalized elution volumes of nitrate ions are plotted versus the Tris buffer concentration, we notice that $V_{\text{tracer}}/V_{\text{column}}$ for the Hypersil MOS particles decreases monotonically with decreasing ionic strength, while elution volumes on the Spherisorb SCX material run into a plateau below a buffer concentration of 0.1 mM. The discrete Donnan exclusion regime with a fully developed plateau can be explained by the significantly higher surface charge density of the Spherisorb SCX particles. This property leads to a much stronger Donnan exclusion of the nitrate ions, in turn enabling the observation of a discrete plateau region (Fig. 5A).

Fig. 5B shows the results of the ISEC calibration. Both curve shapes in this case are similar, in contrast to Fig. 5A, because size-exclusion of the larger polystyrene standards from parts of the interparticle pore space is independent of the surface charge density of the particles and is therefore similar for packing materials with a similar mean particle size and size distribution.

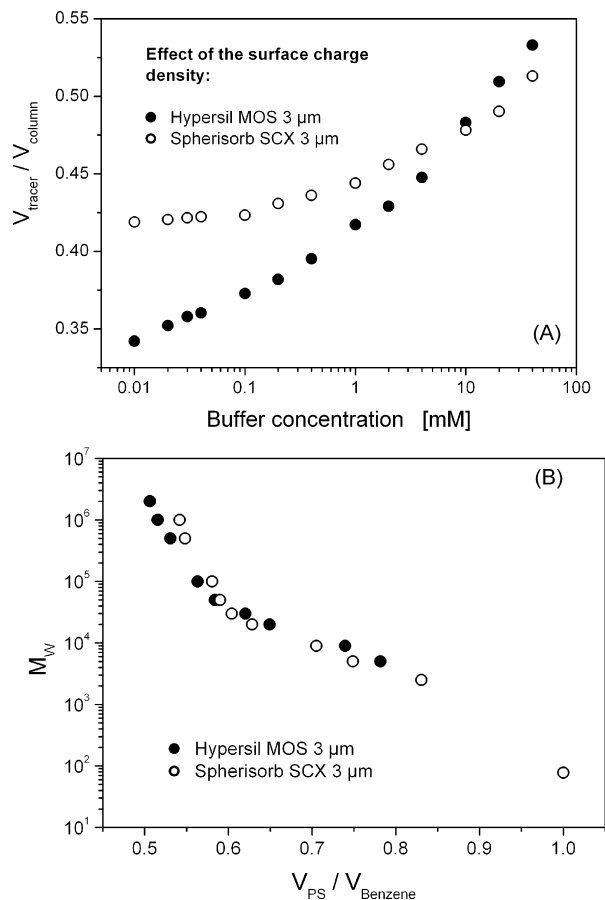


Fig. 5. (A) Electrostatic exclusion curves of nitrate vs. the concentration of Tris-HCl buffer in the mobile phase and (B) inverse size-exclusion curves of polystyrene standards with known molecular weight (M_{W}) for capillaries packed with 3 μm Hypersil MOS (monomeric octyl silica, non-encapped) and 3 μm Spherisorb SCX (propanesulfonic acid-modified silica) particles.

4.3. Effect of the mean intraparticle pore size

Intraparticle co-ion exclusion for a packing material is expected to depend sensitively on the mean pore size, i.e., the actual pore-scale EDL overlap expressed in $r_{\text{pore}}/\lambda_{\text{D}}$ (Fig. 2), assuming that the particle size (cf. Fig. 4) and the surface potential (cf. Fig. 5) of the stationary-phases are identical. To demonstrate the influence of r_{pore} in $r_{\text{pore}}/\lambda_{\text{D}}$, the calibration curves for packed capillaries obtained with Nucleosil 100-5 (5- μm sized particles, nominal 100 \AA pores) and Nucleosil 1000-5 (nominal 1000 \AA pores) are shown in Fig. 6A. The surface charge density of these Nucleosil bare silica particles is higher than that of the Hypersil MOS reversed-phase particles, which leads us to predict a more pronounced plateau region in the Donnan exclusion data for the Nucleosil 100-5 particles (open circles, Fig. 6A) compared to the 10 μm Hypersil MOS particles (open circles, Fig. 4A). This is indeed confirmed by the experimental data when comparing the slopes of both curves at low buffer concentrations. The asymptotic limit of intraparticle exclusion is almost reached at $r_{\text{pore}}/\lambda_{\text{D}}=0.21$ for Nucleosil 100-5 (Fig. 6A), whereas for 10 μm Hypersil MOS (Fig. 4A) the nitrate ions at this ratio still are not completely excluded. The higher surface electrical potential in the even slightly larger pores of the bare silica (162 \AA) compared to the C8-silica material (119 \AA) results in a stronger Donnan exclusion.

In a comparison of columns packed with the Nucleosil 100-5 (162 \AA pores, Table 2) and Nucleosil 1000-5 (1295 \AA pores) particles, the differences in Donnan exclusion are nearly independent

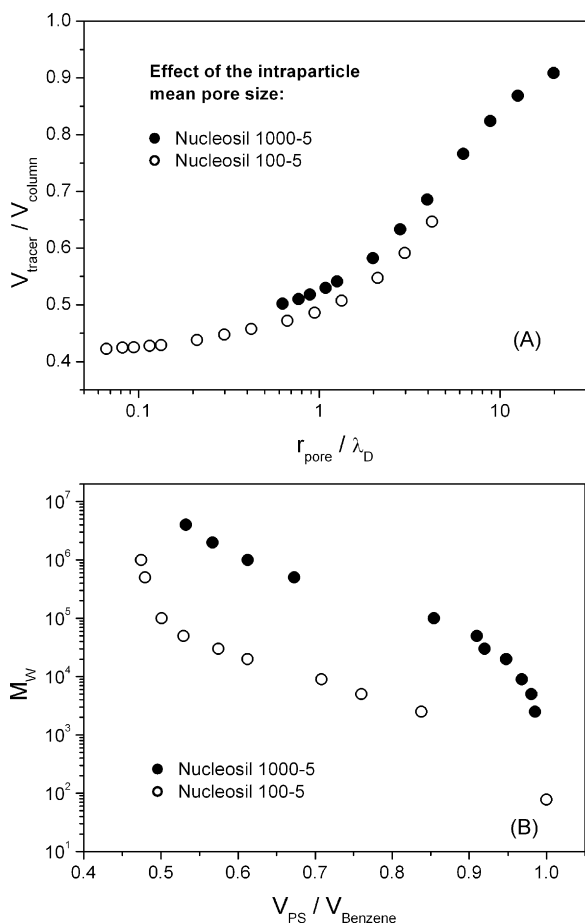


Fig. 6. (A) Electrostatic exclusion curves of nitrate vs. $r_{\text{pore}}/\lambda_D$ and (B) inverse size-exclusion curves of polystyrene standards with known molecular weight (M_w) for capillaries packed with 5 μm Nucleosil 100-5 (100 Å nominal pore size) and Nucleosil 1000-5 bare silica particles (1000 Å).

of the surface electrical potential, but should reflect exclusively the dependence on the mean pore diameter. The much smaller EDL overlap for the Nucleosil 1000-5 particles results in an immediately sharp increase in the $V_{\text{tracer}}/V_{\text{column}}$ data of the Donnan exclusion curve at $r_{\text{pore}}/\lambda_D = 0.63$ (already with the low buffer concentrations), whereas the calibration curve of the Nucleosil 100-5 particles starts much earlier, at $r_{\text{pore}}/\lambda_D = 0.07$ (Fig. 6A). An accurate determination of the point of complete exclusion from the intraparticle pore space cannot be made for the macroporous Nucleosil 1000-5 particles, because the nitrate elution volumes do not reach, but just approach the asymptotic limit (plateau region at still lower values of $r_{\text{pore}}/\lambda_D$ indicating complete Donnan exclusion). Although the slope of the $V_{\text{tracer}}/V_{\text{column}}$ data at buffer concentrations below 0.03 mM ($r_{\text{pore}}/\lambda_D = 1.09$) starts to decrease, the deviation of the calculated $\epsilon_{\text{inter}} = 0.49$ (using the nitrate elution volume with 0.01 mM Tris) from the real packing density is difficult to estimate by extrapolation. Thus, the smallest nitrate elution volume for the macroporous particles at $r_{\text{pore}}/\lambda_D = 0.63$ (lowest Tris buffer concentration used) provides only an upper limit and $\epsilon_{\text{inter}} < 0.49$ (Fig. 6A).

Regarding the analysis of ISEC data for the small-pore and wide-pore silicas (Fig. 6B) a discrete point of complete size-exclusion can be recognized only for the Nucleosil 100-5 particles (open circles) at a molecular weight of 100,000 g/mol translating to the pore diameter of 162 Å in Table 2. For the Nucleosil 1000-5 particles, however, the opposite extreme can be observed: here, the pores are so large to become almost fully penetrated not only by benzene, but also the polystyrene standards with 2500 and 5000 g/mol. A sig-

nificant size-exclusion from the pores starts with 9000 g/mol and reaches the upper limit in this work at 4,000,000 g/mol (translating to a pore diameter of $d_{\text{pore}} = 1948$ Å). Although the point of complete size-exclusion cannot be identified exactly, elution volumes of the 2,000,000 g/mol and 4,000,000 g/mol polystyrene standards are already slightly higher than expected from the linear fit to the data of intermediate-sized polystyrenes indicating the onset of size-exclusion from the interparticle pore space. Thus, the coil diameter of the 2,000,000 g/mol polystyrene standard ($d_{\text{pore}} = 1295$ Å) represents a more reliable pore diameter of the Nucleosil 1000-5 material.

5. Conclusions

Interparticle void volumes (V_{inter}) and porosities (ϵ_{inter}) of particle-packed, 75 μm i.d. fused-silica capillaries have been determined by careful adjustment for complete intraparticle Donnan exclusion of a small, unretained, co-ionic tracer (nitrate ions). Electrostatic exclusion provides a theoretically clear, physically sharp definition of the boundary between (charge-selective) mesopore space and (charge-nonspecific) macropore space in typical hierarchically structured porous media like packed beds and monoliths (Fig. 1).

The operational domain of this approach has been studied for bare silica, reversed-phase, and strong cation-exchange materials with different particle sizes and intraparticle pore sizes. This allowed to realize a wide range of conditions under which this simple approach could be tested by analyzing – in combination with the mobile phase ionic strength (Tris–HCl buffer) – the intraparticle EDL overlap and co-ion exclusion (Fig. 2) in dependence of the intraparticle pore size (Fig. 6) and the surface charge density of the particles (Fig. 5). For all investigated surface chemistries the intraparticle Donnan exclusion approach resulted in values of ϵ_{inter} that agreed well with those obtained independently by ISEC. Limitations to the use of Donnan exclusion (electrostatic exclusion) and ISEC (mechanical exclusion) arise as either type of exclusion becomes noticeable also in the cusp regions between the particles (Fig. 4), or as the intraparticle pores are so large that complete electrostatic and size-exclusion are difficult to realize (Fig. 6).

Because mesoporous packing materials are common in HPLC and a sufficient surface charge density even exists on typical reversed-phase particles (Fig. 4) Donnan exclusion for the determination of ϵ_{inter} presents a most simple, fast, and reliable approach, with convenient mobile phases and detection. It thereby offers advantages compared to ISEC and it also shows that the total pore blocking of reversed-phase packings using a hydrophobic solvent [15] is redundant in most cases, particularly because Cabooter et al. [15] recommended the use of an inorganic salt like NaNO_3 or KI anyway as tracer for the determination of ϵ_{inter} after pore blocking. Our results confirm that the long-known “electrostatic pore blocking” [1] (using just the inorganic salt) is far easier, faster, and not limited by the surface chemistry.

Acknowledgements

This work was supported by an Agilent Technologies Ph.D. Fellowship award through the University Relations Ph.D. Fellowship program. We thank Dr. Uwe Neue (Waters Corporation, Milford, MA) for the gift of the Spherisorb SCX material.

References

- [1] C.A. Rimmer, C.R. Simmons, J.G. Dorsey, J. Chromatogr. A 965 (2002) 219.
- [2] F. Gritti, Y. Kazakevich, G. Guiochon, J. Chromatogr. A 1161 (2007) 157.
- [3] H. Guan, G. Guiochon, J. Chromatogr. A 731 (1996) 27.
- [4] A. Alhedai, D.E. Martire, R.P.W. Scott, Analyst 114 (1989) 869.
- [5] A. Felinger, M. Kele, G. Guiochon, J. Chromatogr. A 913 (2001) 23.

- [6] G. Guiochon, M. Sarker, *J. Chromatogr. A* 704 (1995) 247.
- [7] J.-H. Koh, B.S. Broyles, H. Guan-Sajonz, M.Z.-C. Hu, G. Guiochon, *J. Chromatogr. A* 813 (1998) 223.
- [8] S. Ehlert, T. Rösler, U. Tallarek, *J. Sep. Sci.* 31 (2008) 1719.
- [9] S. Ehlert, K. Kraiczek, J.-A. Mora, M. Dittmann, G.P. Rozing, U. Tallarek, *Anal. Chem.* 80 (2008) 5945.
- [10] F.A.L. Dullien, *Porous Media—Fluid Transport and Pore Structure*, Academic Press, San Diego, CA, 1991.
- [11] H. Rumpf, A.R. Gupta, *Chem.-Ing.-Technol.* 43 (1971) 367.
- [12] I. Halász, K. Martin, *Angew. Chem. Int. Ed.* 17 (1978) 901.
- [13] W.W. Yau, J.J. Kirkland, D.D. Bly, *Modern Size-Exclusion Liquid Chromatography*, John Wiley & Sons, New York, 1979.
- [14] F. Gritti, G. Guiochon, *J. Chromatogr. A* 1136 (2006) 192.
- [15] D. Cabooter, F. Lynen, P. Sandra, G. Desmet, *J. Chromatogr. A* 1157 (2007) 131.
- [16] F. Helfferich, *Ion Exchange*, McGraw-Hill, New York, 1962.
- [17] I. Nischang, G. Chen, U. Tallarek, *J. Chromatogr. A* 1109 (2006) 32.
- [18] A. Höltzel, U. Tallarek, *J. Sep. Sci.* 30 (2007) 1398.
- [19] G.E. Berendsen, P.J. Schoenmakers, L. de Galan, G. Vigh, Z. Varga-Puchony, J. Inczédy, *J. Liq. Chromatogr. Rel. Technol.* 3 (1980) 1669.
- [20] M.J.M. Wells, C.R. Clark, *Anal. Chem.* 53 (1981) 1341.
- [21] H. Engelhardt, H. Müller, B. Dreyer, *Chromatographia* 19 (1984) 240.
- [22] M. Shibukawa, N. Ohta, *Chromatographia* 25 (1988) 288.
- [23] L.G. Daignault, D.C. Jackman, D.P. Rillema, *J. Chromatogr.* 462 (1989) 71.
- [24] F.C. Leinweber, M. Pfaffrodt, A. Seidel-Morgenstern, U. Tallarek, *Anal. Chem.* 77 (2005) 5839.
- [25] T.S. Sørensen (Ed.), *Surface Chemistry and Electrochemistry of Membranes*, Marcel Dekker, New York, 1999.
- [26] H. Strathmann, *Ion Exchange Membrane Separation Processes*, Elsevier, Amsterdam, The Netherlands, 2004.
- [27] S.M. Melnikov, A. Höltzel, A. Seidel-Morgenstern, U. Tallarek, *J. Phys. Chem. C* 113 (2009) 9230.
- [28] R.F. Probst, *Physicochemical Hydrodynamics*, Wiley, New York, 1994.
- [29] P.J. Kemery, J.K. Steehler, P.W. Bohn, *Langmuir* 14 (1998) 2884.
- [30] T.C. Kuo, L.A. Sloan, J.V. Sweedler, P.W. Bohn, *Langmuir* 17 (2001) 6298.
- [31] J.R. Ku, P. Stroeve, *Langmuir* 20 (2004) 2030.
- [32] D. Stein, M. Kruihof, C. Dekker, *Phys. Rev. Lett.* 93 (2004) 035901.
- [33] R. Schmuhl, K. Keizer, A. van den Berg, J.E. ten Elshof, D.H.A. Blank, *J. Colloid Interface Sci.* 273 (2004) 331.
- [34] A. Plecis, R.B. Schoch, P. Renaud, *Nano Lett.* 5 (2005) 1147.
- [35] G. Guiochon, S. Golshan-Shirazi, A.M. Katti, *Fundamentals of Preparative and Nonlinear Chromatography*, Academic Press, Boston, MA, 1994.
- [36] N.S. Pujar, A.L. Zydney, *J. Chromatogr. A* 796 (1998) 229.
- [37] D.B. Burns, A.L. Zydney, *AIChE J.* 47 (2001) 1101.
- [38] D. Gétaz, G. Ströhlein, M. Morbidelli, *J. Chromatogr. A* 1216 (2009) 933.
- [39] F.G. Donnan, *Z. Elektrochem.* 17 (1911) 572.
- [40] F.G. Donnan, E.A. Guggenheim, *Z. Phys. Chem.* 162 (1932) 346.
- [41] J. Ståhlberg, *J. Chromatogr. A* 855 (1999) 3.
- [42] G. Chen, M. Pačes, M. Marek, Y. Zhang, A. Seidel-Morgenstern, U. Tallarek, *Chem. Eng. Technol.* 27 (2004) 417.
- [43] C. Moreau, G. Douhéret, *J. Chem. Thermodyn.* 8 (1976) 403.
- [44] E.F. Casassa, *J. Phys. Chem.* 75 (1971) 3929.
- [45] F. Gritti, A. Cavazzini, N. Marchetti, G. Guiochon, *J. Chromatogr. A* 1157 (2007) 289.
- [46] S. Torquato, *Phys. Rev. Lett.* 74 (1995) 2156.
- [47] J.H. Knox, H.J. Ritchie, *J. Chromatogr.* 387 (1987) 65.
- [48] A. de Klerk, *AIChE J.* 49 (2003) 2022.
- [49] C. Song, P. Wang, H.A. Makse, *Nature* 453 (2008) 629.
- [50] A.V. Anikeenko, N.N. Medvedev, *Phys. Rev. E* 77 (2008) 031101.
- [51] F. Gritti, G. Guiochon, *J. Chromatogr. A* 1166 (2007) 30.